Axisymmetric flame deconvolution using automated Tikhonov regularization

Daun, K. J.; Thomson, Kevin

Combustion Institute Canadian Section, 2006 Spring Technical Meeting [Proceedings], 2006

Axisymmetric Flame Deconvolution using Automated Tikhonov Regularization

K. J. Daun and K. A. Thomson
Institute for Chemical Process and Environmental Technology
National Research Council of Canada

ABSTRACT

When deconvolving data collected in experiments involving axisymmetric flames, small errors that contaminate the data are magnified into large errors in the recovered distribution. Error magnification can be suppressed through Tikhonov regularization although a regularization parameter must first be identified, usually through a time-consuming trial-and-error procedure. This paper presents an algorithm that selects the regularization parameter automatically based on an estimate of the error contaminating the dataset. Solutions obtained using this algorithm are more accurate that those found by onion-peeling and Abel three-point deconvolution. Furthermore, because this algorithm selects the regularization automatically it is faster and easier to implement compared to the traditional trial-and-error regularization approach.

INTRODUCTION

The objective of many experiments involving axisymmetric flames is to deconvolve optical data measured along a set of chord lines passing through the flame field, called the *projected data*, $P(y)$, to recover the radial distribution of a *field variable*, $f(r)$, over the range $0 \le r \le R$, which is shown schematically in Fig. 1 (*a*). These two variables are related by Abel's integral equation,

$$P(y) = 2\int_y^R \frac{f(r)\,r}{\sqrt{r^2 - y^2}}\,dr\,, \tag{1}$$

a type of Volterra integral equation of the first kind. The simplest was of solving Eq. (1) is by onion-peeling. In this procedure the integral domain is first split into N evenly-spaced segments, which is equivalent to discretizing the flame field into N uniformly-spaced annular elements having a radial thickness $\Delta r = R/(N-1/2)$ as shown in Fig. 1 (*b*). By assuming that $f(r)$ is uniform over each sub-domain of r, these values can be extracted from the corresponding integrals, which then contain only geometric terms. Carrying out these integrals transforms Eq. (1) into the $N \times N$ matrix equation $\mathbf{A}_{\mathrm{OP}}\boldsymbol{x} = \boldsymbol{b}$, where $x_i = f(r_i) = f(i\Delta r)$, $b_i = P(y_i) = P(i\Delta r)$, and

$$A_{\mathrm{OP},ij} = \begin{cases} 0, & j < i \\ 2\Delta r\sqrt{\left(j+\tfrac{1}{2}\right)^2 - i^2}, & j = i \\ 2\Delta r\left[\sqrt{\left(j+\tfrac{1}{2}\right)^2 - i^2} - \sqrt{\left(j-\tfrac{1}{2}\right)^2 - i^2}\right], & j > i. \end{cases} \tag{2}$$

This and other popular deconvolution techniques, including Abel three-point deconvolution, are described in greater detail in [1].

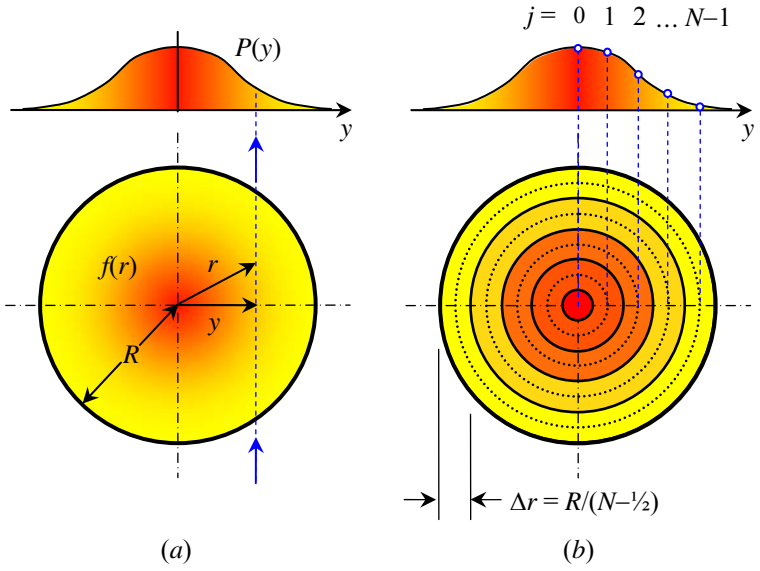

Fig. 1: (*a*) Axisymmetric flame deconvolution and (*b*) discretization of the problem domain.

Traditional deconvolution techniques provide accurate solutions for $f(r)$ when the exact projected data is known. In an experimental setting, however, small errors that contaminate the projected data are magnified by deconvolution into large errors in the recovered field variable distribution. Error amplification is a consequence of the ill-posedness of Abel's integral equation and increases with N, severely limiting the deconvolved field variable resolution. This is demonstrated in the test problem shown in Fig. 2. The field variable was first derived by fitting a 4^{th}-order piecewise polynomial to normalized soot-volume fraction data from a line-of-sight attenuation (LOSA) experiment on a laminar flame [2]. The right-hand side vector $\boldsymbol{b}$, which contains the projected data, was calculated by analytically integrating Eq. (1). This data was contaminated by a perturbation vector $\boldsymbol{\delta b}$ with elements randomly-sampled from an unbiased Gaussian distribution having a standard deviation of 0.01, which is typical of errors encountered in LOSA flame experiments [2]. Figure 2 shows that the small errors contained in $\boldsymbol{\delta b}$ are amplified by onion-peeling and Abel three-point deconvolution into large perturbations in the solution, $\boldsymbol{\delta x}$.

TIKHONOV REGULARIZATION

Error amplification can be suppressed by using regularization to perform the deconvolution. Regularization techniques transform the original ill-posed problem into a set of better-posed or *regularized* problems. Regularized problems that closely resemble the original ill-posed problem are themselves ill-posed, having solutions that solve the original problem with a very small residual but are also highly sensitive to small errors in the input data. Using more regularization improves the solution stability, but at the expense of solution accuracy. The degree of regularization is controlled by a *regularization parameter*, which is adjusted until an acceptable trade-off between solution accuracy and stability is obtained. In a recent work [3], we showed how Tikhonov regularization [4] can be used to perform axial flame deconvolution. In this approach the matrix equation obtained by onion-peeling is augmented by adding a homogeneous system of regularizing equations $\lambda\mathbf{L}$, where λ is a continuously-variable regularization parameter

and $\mathbf{L}$ is a smoothing matrix, which in this problem is an $(N-1\times N)$ matrix that approximates the derivative operator in discrete space [5],

$$\mathbf{L}=\begin{bmatrix} 1 & -1 & 0 & \cdots & & 0 \\ 0 & 1 & -1 & \ddots & & \vdots \\ \vdots & \ddots & \ddots & \ddots & & \\ & & & 1 & -1 & 0 \\ 0 & \cdots & & 0 & 1 & -1 \end{bmatrix}. \tag{3}$$

The regularized solution, $\boldsymbol{x}_\lambda$, is the value of $\boldsymbol{x}$ that minimizes the residual norm of the augmented system of equations, i.e.

$$\left\|\mathbf{A}_\lambda \boldsymbol{x}_\lambda - \boldsymbol{b}_\lambda\right\|_2 = Min_x\left(\left\|\mathbf{A}_\lambda \boldsymbol{x} - \boldsymbol{b}_\lambda\right\|_2\right) = Min_x\left(\left\|\begin{bmatrix}\mathbf{A}\\ \lambda\mathbf{L}\end{bmatrix}\boldsymbol{x} - \begin{bmatrix}\boldsymbol{b}\\ 0\end{bmatrix}\right\|_2\right), \tag{4}$$

which can be found efficiently by solving

$$\left(\mathbf{A}_{\mathrm{OP}}^T\mathbf{A}_{\mathrm{OP}} + \lambda^2\mathbf{L}^T\mathbf{L}\right)\boldsymbol{x} = \mathbf{A}_{\mathrm{OP}}^T\boldsymbol{b}. \tag{5}$$

In our previous paper [3] we showed that λ can be adjusted with high fidelity until a near-optimum trade-off between accuracy and solution stability is found for a given field distribution, level of discretization, and degree of error contamination. Strategies for selecting λ are presented in the next section.

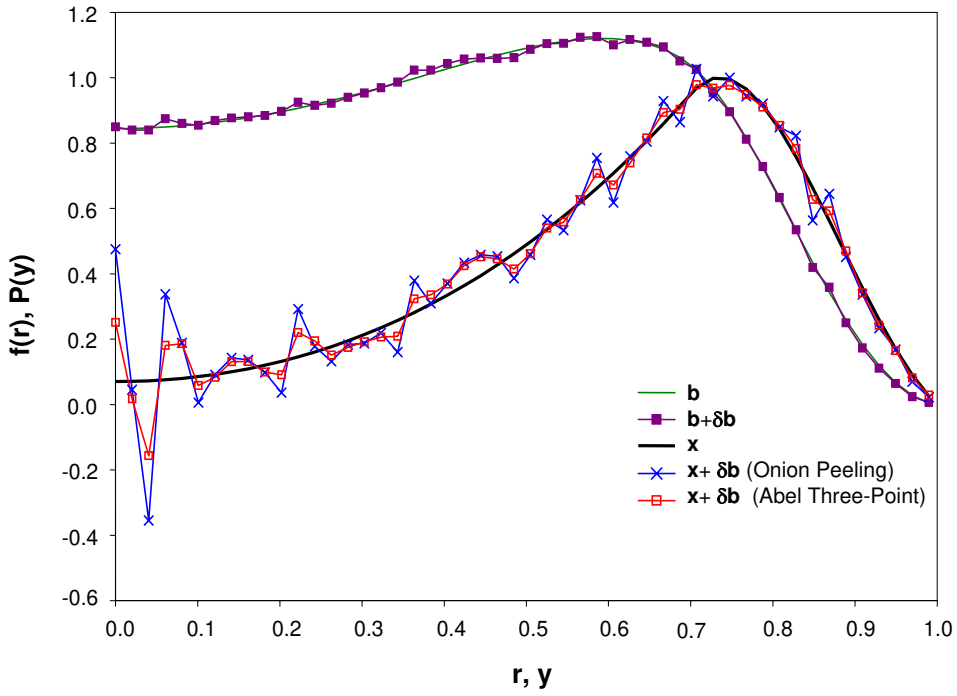

Fig. 2: Example LOSA deconvolution problem showing error amplification by deconvolution. (Based on experimental data from [2].)

SELECTING THE REGULARIZATION PARAMETER

When selecting the regularization parameter, the goal is to minimize the overall solution error, which is due to both the contamination of the projected data and to the regularization process. Formally, the total error is written as [6]

$$\boldsymbol{x} - \boldsymbol{x}_\lambda^{pert} = \mathbf{A}_{\mathrm{OP}}^{-1}\boldsymbol{b} - \mathbf{A}_\lambda^{-1}\boldsymbol{b}^{pert} = \left(\mathbf{A}_{\mathrm{OP}}^{-1} - \mathbf{A}_\lambda^{-1}\right)\boldsymbol{b} - \mathbf{A}_\lambda^{-1}\boldsymbol{\delta b}, \tag{5}$$

where $\boldsymbol{x}$ denotes the exact, unperturbed solution, $\boldsymbol{b}^{pert} = \boldsymbol{b}+\boldsymbol{\delta b}$, $\boldsymbol{x}_\lambda^{pert} = (\boldsymbol{x}+\boldsymbol{\delta x})_\lambda$ is the regularized solution of the perturbed matrix equation, and $\mathbf{A}_{\mathrm{OP}}{}^{-1}$ and $\mathbf{A}_\lambda{}^{-1}$ are the pseudoinverses of the onion-peeling and augmented matrices, respectively. The total error is more easily quantified by taking the l_2-norm of the vectors in Eq. (5),

$$\varepsilon_{tot}(\lambda) = \left\|\boldsymbol{x} - \boldsymbol{x}_\lambda^{pert}\right\|_2 \le \left\|\left(\mathbf{A}_{OP}^{-1} - \mathbf{A}_\lambda^{-1}\right)\boldsymbol{b}\right\|_2 + \left\|\mathbf{A}_\lambda^{-1}\boldsymbol{\delta b}\right\|_2 = \varepsilon_{reg}(\lambda) + \varepsilon_{pert}(\lambda), \tag{6}$$

where $\varepsilon_{reg}(\lambda)$ is the regularization error and $\varepsilon_{pert}(\lambda)$ is the perturbation error. As described above, increasing λ suppresses the magnification of $\boldsymbol{\delta b}$ and decreases $\varepsilon_{pert}(\lambda)$, but this also increases the $\varepsilon_{reg}(\lambda)$ since $\lambda\mathbf{L}$ obscures $\mathbf{A}_{\mathrm{OP}}$ in the augmented matrix $\mathbf{A}_\lambda$ as λ becomes large. Thus, a value of λ must be chosen that is an acceptable trade-off between $\varepsilon_{pert}(\lambda)$ and $\varepsilon_{reg}(\lambda)$.

Most often, λ is selected heuristically with the aid of an L-curve [3, 6], a plot of the smoothed solution norm against the residual norm for solutions obtained using different values of λ. This curve is shown in Fig. 3 for the problem described above with $N = 50$. Although solutions on the far-left side of the curve have a small residual, $\|\mathbf{A}_{\mathrm{OP}}\boldsymbol{x}_\lambda^{pert} - \boldsymbol{b}^{pert}\|_2$, they are *under-regularized* since their large solution norm, $\|\mathbf{L}\boldsymbol{x}_\lambda^{pert}\|_2$, shows that they are contaminated with large perturbations. Solutions become smoother as λ increases, but those on the far-right side of the curve are *over-regularized* because they no longer satisfy the original ill-posed problem as indicated by their large residual. The best trade-off between smoothness and accuracy is usually found by visually inspecting the solutions that lie near the corner of the L-curve, a time-consuming process that demands specialized knowledge of regularization on the part of the analyst.

A more sophisticated way of choosing λ is based on the observation that, since $\varepsilon_{reg}(\lambda)$ and $\varepsilon_{pert}(\lambda)$ increase and decrease in a monotonic way with increasing λ, these errors can be balanced by using the value of λ that satisfies $\varepsilon_{reg}(\lambda^*) = \varepsilon_{pert}(\lambda^*)$. Unfortunately, λ^* cannot normally be found using Eq. (6) directly, since $\boldsymbol{b}^{pert}$ is known rather than $\boldsymbol{b}$ and $\boldsymbol{\delta b}$ individually. An estimate of $\|\boldsymbol{\delta b}\|_2$ is often available, however, usually from the variance of independently-measured sets of projected data. If this is the case $\lambda^\dagger$ can be approximated using the *discrepancy principle* [6, 7], which states that λ should be chosen so that

$$\left\|\mathbf{A}_{\mathrm{OP}}\boldsymbol{x}_\lambda^{pert} - \boldsymbol{b}^{pert}\right\|_2 = \delta_e \ge \left\|\boldsymbol{\delta b}\right\|_2, \tag{7}$$

where δ_e is most often set equal to $\|\boldsymbol{\delta b}\|_2$. The left- and right-hand sides of Eq. (16) are estimates of the regularization and perturbations error, respectively, projected into the vector space of $\boldsymbol{b}$.

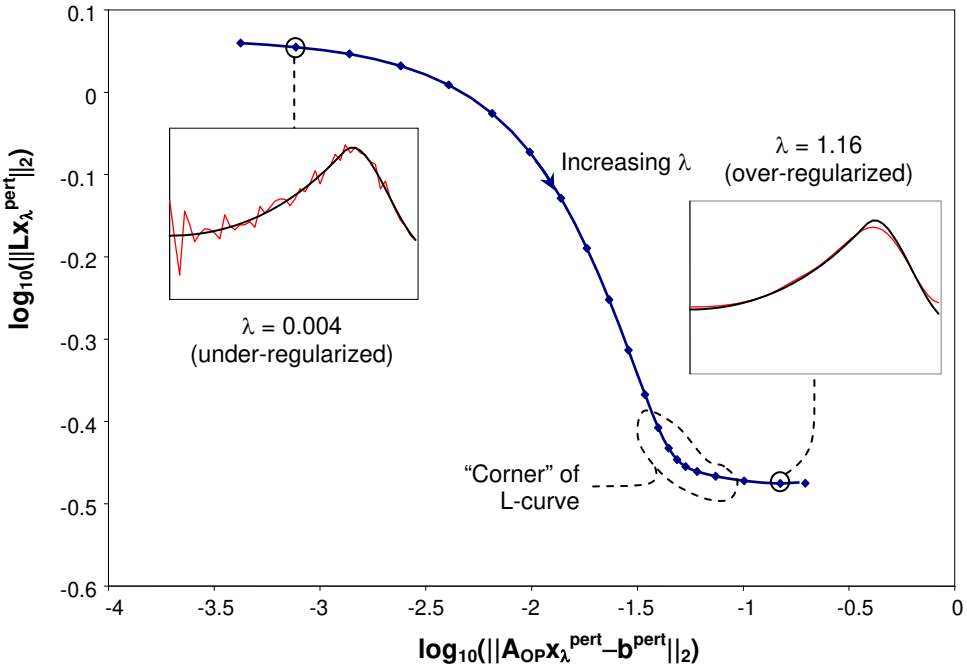

Fig. 3: L-curve for the LOSA deconvolution problem shown in Fig. 2, with $N = 50$.

DEMONSTRATION OF METHOD

The performance of the Tikhonov auto-regularization method described above is compared to that of onion-peeling and Abel three-point deconvolution by solving the LOSA problem shown in Fig. 2. In order to simulate an experimental environment, the projected data is contaminated with error randomly-sampled from an unbiased Gaussian distribution having a standard deviation of $0.01\sqrt{20}$. Each element of the perturbed dataset, $\boldsymbol{b}^{pert}$, is set equal to the average of 20 independent samples, and the corresponding standard deviation of the mean, σ_m, is given by $\sigma/\sqrt{20}$, where σ is the standard deviation of the sampled data. The expected value of σ_m is 0.01, which is typical for LOSA experiments carried out on laminar flames [2].

The performance of the deconvolution algorithms is measured using the root-mean-squared error of the recovered field distributions,

$$\varepsilon_{\mathrm{RMS}} = \frac{\left\| \boldsymbol{x}^{pert} - \boldsymbol{x} \right\|_2}{\sqrt{N}}, \tag{8}$$

obtained using different numbers of projections, N. At each value of N, 20 independent sets of projected data are supplied to the deconvolution algorithms. The Tikhonov regularization parameter is calculated automatically for each dataset by substituting an estimate of $\|\boldsymbol{\delta b}\|_2$,

$$\left\| \boldsymbol{\delta b} \right\|_2 \approx \sqrt{N}\sigma_m = \sqrt{\frac{N}{20}}\sigma, \tag{9}$$

into Eq. (7), which in turn is solved for λ using a safeguarded secant root-finding algorithm [5]. The averages of the resulting $\varepsilon_{\mathrm{RMS}}$ values are plotted in Fig. 4, which shows that the solutions found using Tikhonov auto-regularization are superior to those found with onion-peeling and Abel three-point deconvolution over the whole range of N. In fact, the root-mean-squared errors

of the Tikhonov solutions actually decrease with increasing N, because the perturbation error is suppressed to the extent that the dominant error in the Tikhonov solutions is caused by assuming a uniform $f(r)$ over each element, which in turn diminishes with increasing N.

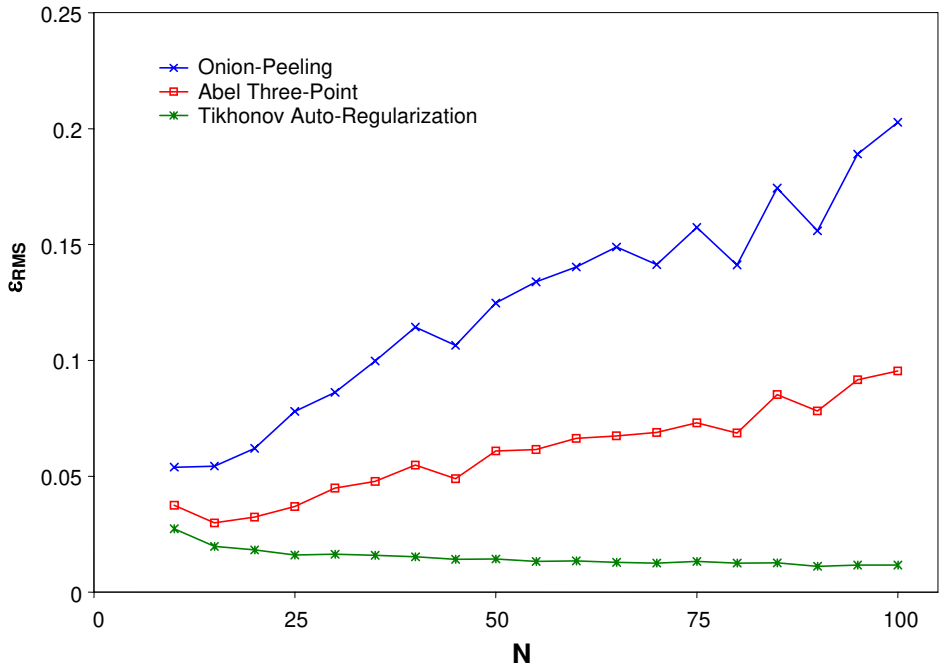

Fig. 4: Accuracy of field distributions obtained using different deconvolution techniques.

CONCLUSIONS

Tikhonov regularization is an effective way of solving flame deconvolution problems in which the projected data is contaminated with error. Implementation of this technique is complicated, however, by the fact that a regularization parameter must first be specified. This paper presented an algorithm for automatically selecting this value using the discrepancy principle. Tikhonov auto-regularization provides more accurate solutions than onion-peeling and Abel three-point deconvolution, and furthermore, because the regularization parameter is selected automatically, this technique is easier to implement than is the case when this value is found manually.

REFERENCES

[1] Dasch, C. J., Applied Optics 31:1146 (1992).

[2] Thomson, K. A., Güilder, Ö. L., Weckman, E. J., Fraser, R. A., Smallwood, G. J., and Snelling, D. R., Comb. Flame 140:222 (2005).

[3] Daun, K. J, Thomson, K. A., Liu, F. and Smallwood, G. J, Applied Optics (in press)

[4] Tikhonov, A. N., J. Eng. Phys. 29:816 (1975).

[5] Press, W. H., Teuklosky, S. A., Vetterling, W. T., and Flannery, B. P., Numerical Recipes in C: The Art of Scientific Computing, 2nd Ed., Cambridge University Press, 2002.

[6] Hansen, P. C., Rank-Deficient and Discrete Ill-Posed Problems: Numerical Aspects of Linear Inversion, SIAM, 1998.

[7] Morozov, V. A., Soviet Math. Dokl 7:414 (1966), as reported in [6].